Vibration and Stability Analysis of Multi Walled Piezoelectric Nanoresonator

Sayyid H. HASHEMI KACHAPI

Researcher, Department of Mechanical Engineering, Babol Noshirvani University of Technology, P.O. Box484, Shariati Street, Babol, Mazandaran47148-71167, Iran, sha.hashemi.kachapi@gmail.com

Abstract: - In this work, vibration and stability analysis of multi walled piezoelectric nanoresonator (MWPENR) based on cylindrical nano-shell is investigated using the Gurtin–Murdoch surface/interface theory and also other nonclassical theories such as nonlocal (NLT) and nonlocal strain gradient (NSGT) approaches. The nanoresonator is embedded in visco-Pasternak medium, the nonlinear van der Waals (vdW) and electrostatic forces. Hamilton's principle is used for deriving of the governing equations and boundary conditions and also the assumed mode method is used for changing the partial differential equations into ordinary differential equation. The influences of the surface/interface effect, piezoelectric voltage, boundary conditions, the length to radius ratio, the nanoresonator gap width and other parameters are studied on the frequency and stability analysis of MWPENR. It is found that in all boundary conditions, higher surface/interface densities leads to reduction of MWPENR stiffness, as a result cause to decreasing of the dimensionless natural frequency and pull in voltage compared to case of without S/I effects. Also, with increasing of b/R_3 ratio and the piezoelectric voltage $\bar{V}_p$, and decreasing of L/R_3 ratio, due to increasing of MWPENR stiffness, the pull-in voltages of the piezoelectric nanoresonator is increased.

Keywords: - Multi walled piezoelectric nanoresonator; Gurtin–Murdoch surface/interface theory; Nonlocal strain gradient; Stability analysis, electrostatic excitation; Visco-Pasternak medium; Van der Waals force.

Nomenclature: Notation and symbols

symbols	Description	symbol	Description
h_{Nn}	Thickness of nanoshell (NS)	h_{pn}	Piezoelectric layer thickness
L	piezoelectric nanoshell Length	E_{pn}	Young modulus of piezoelectric layer
R_n	The mid-surface radius	υ_{pn}	Poisson ratio of piezoelectric layer
x	Axial direction	ρ_p	Mass density of piezoelectric layer
θ	Circumferential direction	e_{31pn}, e_{32pn}	Piezoelectric constants
z	Radius direction	η_{33pn}	Dielectric constant
E_{Nn}	Young modulus of nanoshell	s_{kn}	Piezoelectric inner and outer surface
υ_{Nn}	Poisson ratio of nanoshell	$\lambda^{s_{kn}}, \mu^{s_{kn}}$	Lamé's constants of piezoelectric layer
ρ_{Nn}	Mass density of nanoshell	$\bar{E}_{pn}$	Electric field
I_{kn}	Nanoshell Inner and outer surface	D_{zpn}	Electric displacement
$\lambda^{I_{k(n)}}, \mu^{I_{k(n)}}$	Lamé's constants of nanoshell	$\tau_0^{s_{kn}}$	Residual stress of piezoelectric layer
$\tau_0^{I_{k(n)}}$	Residual stress of nanoshell	$e_{31pn}^{s_k}, e_{32pn}^{s_k}$	Surface piezoelectric constants
$\rho^{I_{k(n)}}$	Nanoshell interface mass density	$\rho^{s_{kn}}$	Piezoelectric surface mass density
C_{ijNn}	Elastic constant of nanoshell	C_{ijpn}	Elastic constant of piezoelectric layer
σ_{ijNn}	Middle stress of nanoshell	σ_{ijpn}	Middle stress of piezoelectric layer
$\kappa_{(x,\theta)}$	Curvature components	V_{pn}	Piezoelectric voltage
$\varepsilon_{(x,\theta)}^0, \gamma_{x\theta}^0$	Middle surface strains	π_n	Total strain energy
u	Displacement of x direction	T_n	Total kinetic energy
v	Displacement of θ direction	I_n	Mass moments of inertia
w	Displacement of z direction	C_{wn}	Damping coefficient

symbols	Description	symbol	Description
∇	Laplace operator	K_{wn}	Winkler modulus
ω	Natural frequency	K_{pn}	Pasternak Shear modulus
M	Total mass matrix	W_n	Total work
C	Total damping coefficient	K_n	Total stiffness matrix
$\bar{F}$	Loads by piezoelectric voltage	b_n	The nanoresonator gap width
V_{DnC}	direct electric voltage	$\bar{C}_{vdwn}^{L}$	Linear van der Waals coefficient
$\bar{C}_{vdwn}^{NL}$	Nonlinear van der Waals coefficient	μ	Nonlocal scale parameter
η	Material length scale parameter		

1. INTRODUCTION

Piezoelectric materials are widely used in modern engineering due to its direct and inverse effects and play an important role for nano structures such as nanomechanical resonators [1-3]. On the other hand, due to excessive use of nanoresonator, especially piezoelectric nanoresonator in vibration devices, modeling their mathematical modeling and vibration behaviors are essential. In spite of a large number of studies on nano resonators dynamics, just a very small number of these works is related to the analysis of vibration and stability analysis of piezoelectric nanoresonator based on multi walled nano shell (MWNS) that are structurally built by multi concentric single-walled nano shell (SWNS) and those mechanical properties are superior to the mechanical properties of SWNS. As a result, MWNSs are preferred, in some applications such as nanoresonator. Also, as behavior of nanostructures, is greatly affected by their surface parameters and the results of the experimental observation show that the existence of surface and the size dependent effects are crucial for precisely determining the size-dependent parameters of the nano-structures which should be included in theoretical models. For this reason, surface/interface elasticity, which was brought up by Gurtin and Murdoch, is taken into consideration [4].

Many studies have been carried out on the vibration and stability analysis of nanostructure that some of them are reviewed here. Hajnayeb and Khadem studied forced vibrations of a double-walled carbon nanotube (DWNT) subjected to an electrostatic actuation and the nonlinear form of the interlayer van der Waals (vdW) force [5]. In this work, the frequency response, stability analysis and bifurcation points are obtained. Also, based on nonlocal piezoelasticity cylindrical shell theory, Ghorbanpour Arani et al. studied nonlinear vibration and instability of the embedded double walled boron nitride nanotubes conveying viscous fluid and electro-thermo-mechanical buckling of double-walled boron-nitride nanotube (DWBNNT) embedded in bundle of CNTs [6, 7]. Tadi Beni et al. investigated on pull-in behavior of nanostructures using nonclassical theories such as modified couple stress theory [8]. Recently, Hashemi Kachapi et al. presented Gurtin–Murdoch surface/interface theory to investigate the effects of the surface/interface energy on the linear and nonlinear vibration and stability analysis of piezoelectric nanostruacures [9-14]. They showed that increasing or decreasing of surface/interface parameters lead to increasing or decreasing the natural frequency, resonance amplitude, resonant frequency, the system's instability, nonlinear behavior and bandwidth. Nonlinear transient isogeometric and bending and buckling analyses are investigated by Phung-Van, Thanh and etc. on micro and nano plates and shells based on nonclassical theories [15-21].

To the best knowledge of the author that Gurtin–Murdoch surface/interface theory and also other nonclassical theories such as nonlocal (NLT) and nonlocal strain gradient (NSGT) approaches are used to investigate vibration and stability analysis of multi walled piezoelectric nanoresonator (MWPENR) subjected to visco-Pasternak medium, the nonlinear van der Waals (vdW) and electrostatic forces has not been studied yet. In current study. For this purpose, Hamilton's principle and the assumed mode method combined with Lagrange–Euler's is used to achieve influences of the surface/interface effect, piezoelectric voltage, boundary conditions, the length to radius ratio, the nanoresonator gap width and other parameters on the frequency and stability analysis of MWPENR.

2. MATHEMATICAL FORMULATION

A schematic diagram of multi walled piezoelectric nanoresonator embedded with two piezoelectric layers and visco-Pasternak medium in outer layer is shown in Figure 1 (a-c). The geometrical parameters of the cylindrical shell are the length L, the mid-surface radius R_n with nano shell thickness $2h_{Nn}$ and coated by two piezoelectric layers with total thickness $2h_{pn}$ for the outer walled and also the mid-surface radius R_{k+1} and nano shell thickness $2h_{N(k+1)}$ for the other inner walled layers.

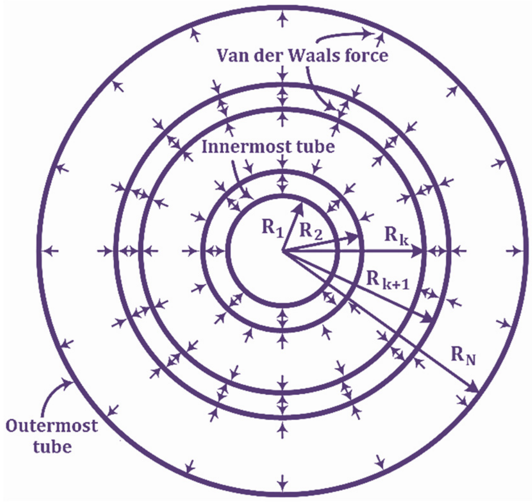

(a) Illustration of vdW forces between two adjacent tubes of a multiple shell cross section of a multi walled carbon nanotube (MWCNT)

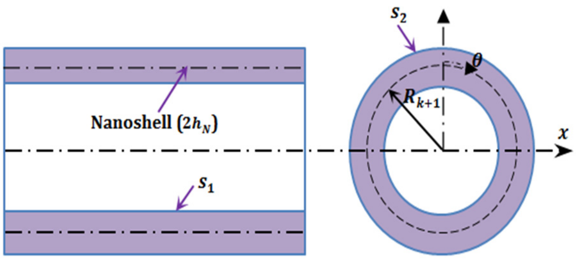

(b) Modelling of 1 ... $k+1$ tube of MWCNT as a nanoresonator with surface model

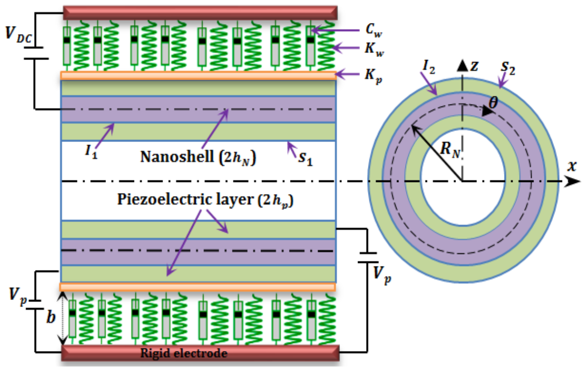

(c) Modelling of last tube of MWCNT as a piezoelectric nanoresonator with surface/interface model

Figure. 1. Multi walled piezoelectric nanoresonator (MWPENR) based on cylindrical nano-shell

2.1. Non- classical shell theory

Based on the Gurtin–Murdoch surface/interface elasticity theory, the normal stresses σ_{xx} and $\sigma_{\theta\theta}$ can be written as [4, 9-14]

$$\sigma_{xx(N,p)} = C_{11(N,p)}\varepsilon_{xx} + C_{12(N,p)}\varepsilon_{\theta\theta} -e_{31p}\bar{E}_{xp} + \frac{\upsilon_{(N,p)}\sigma_{zz(N,p)}}{1-\upsilon_{(N,p)}}, \tag{1}$$

$$\sigma_{\theta\theta(N,p)} = C_{21(N,p)}\varepsilon_{xx} + C_{22(N,p)}\varepsilon_{\theta\theta} -e_{32p}\bar{E}_{\theta p} + \frac{\upsilon_{(N,p)}\sigma_{zz(N,p)}}{1-\upsilon_{(N,p)}}, \tag{2}$$

$$\sigma_{x\theta(N,p)} = C_{66(N,p)}\gamma_{x\theta}, \tag{3}$$

where based on nonclassical continuum model, σ_{zz} is expressed as following

$$\sigma_{zz} = \frac{z}{h_{Nn}+h_{p2}}\left(\begin{array}{c}\left(\tau_0^{ps}+\tau_0^{NI}\right)\times \\ \left(\dfrac{\partial^2 w}{\partial x^2}+\dfrac{1}{R^2}\dfrac{\partial^2 w}{\partial\theta^2}\right) \\ -\left(\rho^{ps}+\rho^{NI}\right)\dfrac{\partial^2 w}{\partial t^2}\end{array}\right), \tag{4}$$

in all following formulations, all of the piezoelectric parameters (the materials and geometrical parameters) are neglected for first layer and to be zero and all of the materials and geometrical parameters of nanoshell in the first layer are similar to the second layer of nanostructure.

Also all coefficients and phrases of Eqs. (1)- (4) such as nonlinear deflection, displacement fields and curvatures, relations of Gurtin–Murdoch surface/interface elasticity theory and etc. can be expressed in full detail in reference [11-14, 22-27].

2.2. GOVERNING EQUATIONS

In this section, at first the governing equations of motion of the piezoelectric cylindrical nanoshell are obtained by applying the Hamilton's principle, and then discretized form of the equation of motion is obtained by applying the assumed mode method and combination of Lagrange- Euler's equations. The total strain energy considering the TWPENR with surface stress effect is expressed as:

$$\begin{aligned}\pi_n &= \frac{1}{2}\int_0^L\int_0^{2\pi}\int_{-h_N}^{h_N}\sigma_{ijN}\varepsilon_{ij}\,Rdzd\theta dx \\ &+\frac{1}{2}\int_0^L\int_0^{2\pi}\int_{h_N}^{h_N+h_p}\left(\begin{array}{c}\sigma_{ijp}\varepsilon_{ij} \\ -\bar{E}_{zp2}D_{zp}\end{array}\right)Rdzd\theta dx \\ &+\frac{1}{2}\int_0^L\int_0^{2\pi}\left(\begin{array}{c}\left(\sigma_{ij}^{s_2}\varepsilon_{ij}-\bar{E}_{zp}D_i^{s_2}\right)\times \\ \left(R+h_N+h_p\right)\end{array}\right)d\theta dx \\ &+\frac{1}{2}\int_0^L\int_0^{2\pi}\sigma_{ij}^{s_1}\varepsilon_{ij}\,(R-h_N)d\theta dx = \\ &\frac{1}{2}\int_0^L\int_0^{2\pi}\left\{\begin{array}{c}N_{xxn}\varepsilon_{xx}^0+N_{\theta\theta n}\varepsilon_{\theta\theta}^0+ \\ N_{x\theta n}\gamma_{x\theta}^0+M_{xxn}\kappa_{xx}+ \\ M_{\theta\theta n}\kappa_{\theta\theta}+M_{x\theta n}\kappa_{x\theta} \\ +\eta_{33}\bar{E}_{zp}^2h_p\end{array}\right\}R_n d\theta dx\end{aligned} \tag{5}$$

In Eq. (5), the forces (N) and moment (M) resultants are defined in Hashemi Kachapi et al. [12] for SWPENR. And, as explained, all the sentences mentioned in reference [12] belong to the last wall (in this article, the third wall), which is considered a nanoshell with two piezoelectric layers, and in the other walls (in this article, the first and second walls) are not considered piezoelectric effects.

The kinetic energy of the nanoshell may be written as:

$$T_n=\frac{1}{2}\iint I_n\begin{pmatrix}\left(\frac{\partial u_n}{\partial t}\right)^2\\+\left(\frac{\partial v_n}{\partial t}\right)^2\\+\left(\frac{\partial w_n}{\partial t}\right)^2\end{pmatrix}R_n d\theta dx \tag{6}$$

where

$$I_n=\int_{-h_N}^{h_N}\rho_N\,dz+\int_{-h_N-h_p}^{-h_N}\rho_p\,dz+\int_{h_N}^{h_N+h_p}\rho_p\,dz+\rho^{S,I}=2\rho_N h_N+2\rho_p h_p+2\rho^{ps}+2\rho^{NI}$$

The work done by the surrounded viscoelastic medium including the visco-Pasternak medium and viscous damping and also the nonlinear van der Waals interaction and the nonlinear electrostatic force for example for three walled piezoelectric nanoresonator (TWPENR), respectively, can be expressed as [9-14, 28, 29] where I made in my previous works:

$$W_{vdw}=\int_0^L\int_0^{2\pi}\int_0^{w_1}\begin{pmatrix}C^L_{vdw(12)}\times\\(w_2-w_1)\\+C^{NL}_{vdw(12)}\times\\(w_2-w_1)^3\end{pmatrix}dw_1\,R_1 d\theta dx+\int_0^L\int_0^{2\pi}\int_0^{w_2}\begin{pmatrix}C^L_{vdw(23)}\times\\(w_3-w_2)\\+C^{NL}_{vdw(23)}\times\\(w_3-w_2)^3\\-\left(\frac{R_1}{R_2}\right)\times\\\begin{pmatrix}C^L_{vdw(12)}\times\\(w_2-w_1)\\+C^{NL}_{vdw(12)}\times\\(w_2-w_1)^3\end{pmatrix}\end{pmatrix}dw_2R_2d\theta dx \tag{7}$$
$$-\int_0^L\int_0^{2\pi}\int_0^{w_3}\left(\frac{R_2}{R_3}\right)\times\begin{pmatrix}C^L_{vdw(32)}\times\\(w_3-w_2)+\\C^{NL}_{vdw(32)}\times\\(w_3-w_2)^3\end{pmatrix}dw_3\,R_3d\theta dx,$$

$$W_{vm}=-\int_0^L\int_0^{2\pi}\int_0^{w_3}\begin{pmatrix}K_w w_3\\-K_p\nabla^2 w_3\\+C_w\frac{\partial w_3}{\partial t}\end{pmatrix}dw_3R_3d\theta dx, \tag{8}$$

$$W_e=\int_0^L\int_0^{2\pi}\int_0^{w_3}\frac{(\pi\Upsilon(V_{DC}+V_{AC}\cos(\omega t))^2)\times dw_3R_3d\theta dx}{\sqrt{(b_2-w_3)\times(2R_3+b_3-w_3)}\times\left[\cosh^{-1}\left(1+\frac{b_3-w_3}{R_3}\right)\right]^2}, \tag{9}$$

where all coefficients and phrases of Eqs. (7)- (9) can be seen in references [9-14] where I made in my previous works. The equations of motion and corresponding boundary conditions of the piezoelectric shell can be derived from Hamilton's principle

$$\int_0^t\begin{pmatrix}\delta T_n-\delta\pi_n+\delta w_{vm}\\+\delta w_{vdw}+\delta w_e\end{pmatrix}dt=0, \tag{10}$$

and substituting Eqs. (5)- (10) into it, the governing equations of motion and boundary conditions for TWPENR respectively are obtained as follows:

$$\delta u_n:\quad \frac{\partial N_{xn}}{\partial x}+\frac{1}{R_n}\frac{\partial N_{x\theta n}}{\partial\theta}=I_n\frac{\partial^2 u_n}{\partial t^2}, \tag{11}$$

$$\delta v_n:\quad \frac{\partial N_{x\theta n}}{\partial x}+\frac{1}{R_n}\frac{\partial N_{\theta n}}{\partial\theta}=I_n\frac{\partial^2 v_n}{\partial t^2}, \tag{12}$$

$$\begin{aligned}\delta w_n:\quad &\frac{\partial^2 M_{xn}}{\partial x^2}+\frac{2}{R_n}\frac{\partial^2 M_{x\theta n}}{\partial x\partial\theta}+\frac{1}{R_n^2}\frac{\partial^2 M_{\theta n}}{\partial\theta^2}-\frac{N_{\theta n}}{R_n}+N_{xn}\frac{\partial^2 w_n}{\partial x^2}\\&+\frac{\partial N_{xn}}{\partial x}\frac{\partial w_n}{\partial x}+\frac{N_{\theta n}}{R_n^2}\frac{\partial^2 w_n}{\partial\theta^2}+\frac{1}{R_n^2}\frac{\partial N_{\theta n}}{\partial\theta}\frac{\partial w_n}{\partial\theta}+\frac{2}{R_n}N_{x\theta n}\frac{\partial^2 w_n}{\partial x\partial\theta}\\&+\frac{1}{R_n}\frac{\partial N_{x\theta n}}{\partial x}\frac{\partial w_n}{\partial\theta}+\frac{1}{R_n}\frac{\partial N_{x\theta n}}{\partial\theta}\frac{\partial w_n}{\partial x}\\&=I_n\frac{\partial^2 w_n}{\partial t^2}+S_n-\frac{\pi\Upsilon(V_{DC}+V_{AC}\cos(\omega t))^2}{\sqrt{(b_2-w_2)(2R_2+b_2-w_2)}\times\left[\cosh^{-1}\left(1+\frac{b_2-w_2}{R_2}\right)\right]^2},\end{aligned} \tag{13}$$

where S_n for the inner and outer layer, respectively, are:

$$S_1=-\begin{pmatrix}C^L_{vdw(12)}(w_2-w_1)\\+C^{NL}_{vdw(12)}(w_2-w_1)^3\end{pmatrix},) \tag{14a}$$

$$S_2=\begin{pmatrix}-C^L_{vdw(23)}(w_3-w_2)\\-C^{NL}_{vdw(23)}(w_3-w_2)^3\\+\left(\frac{R_1}{R_2}\right)\begin{pmatrix}C^L_{vdw(12)}(w_2-w_1)\\+C^{NL}_{vdw(12)}(w_2-w_1)^3\end{pmatrix}\end{pmatrix} \tag{14b}$$

$$S_3 = \left(\begin{array}{c}\left(\frac{R_2}{R_3}\right)\left(\begin{array}{c}C^L_{vdw(32)}(w_3-w_2)\\+C^{NL}_{vdw(32)}(w_3-w_2)^3\end{array}\right)\\+K_w w_3 - K_p\nabla^2 w_3 + C_w\frac{\partial w_3}{\partial t}\end{array}\right) \tag{14c}$$

and boundary conditions are obtained as follows:

$$\delta u_n = 0 \;\; or \;\; N_{xn}n_x + \frac{1}{R_n}N_{x\theta n}n_\theta = 0, \tag{15a}$$

$$\delta v_n = 0 \;\; or \;\; N_{x\theta n}n_x + \frac{1}{R_n}N_{\theta n}n_\theta = 0, \tag{15b}$$

$$\delta w_n = 0 \;\; or \;\; \left(\begin{array}{c}\frac{\partial M_{xn}}{\partial x}+\frac{1}{R_n}\frac{\partial M_{x\theta n}}{\partial \theta}\\+N_{xx}\frac{\partial w_n}{\partial x}+\frac{N_{x\theta}}{R_n}\frac{\partial w_n}{\partial \theta}\end{array}\right)n_x + \left(\begin{array}{c}\frac{1}{R_n}\frac{\partial M_{x\theta n}}{\partial x}+\frac{1}{R_n^2}\frac{\partial M_{\theta n}}{\partial \theta}\\+\frac{N_{x\theta n}}{R_n}\frac{\partial w_n}{\partial x}+\frac{N_{\theta n}}{R_n^2}\frac{\partial w_n}{\partial \theta}\end{array}\right)n_\theta = 0, \tag{15c}$$

$$\frac{\partial w_n}{\partial x} = 0 \;\; or \;\; M_{xn}n_x + \frac{1}{R_n}M_{x\theta n}n_\theta = 0, \tag{15d}$$

$$\frac{\partial w_n}{\partial \theta} = 0, or \;\; \frac{1}{R_n}M_{x\theta n}n_x + \frac{1}{R_n^2}M_{\theta n}n_\theta = 0, \tag{15e}$$

The following dimensional parameters are also used to dimensionless equations of motion and boundary conditions.

$$\begin{gathered}
\bar{u}_n = \frac{u_n}{h_{Nn}}, \bar{v}_n = \frac{v_n}{h_{Nn}}, \bar{w}_n = \frac{w_n}{h_{Nn}},\\
\xi_n = \frac{x_n}{L}, \bar{b}_n = \frac{b_n}{L}, \bar{A}_{ijNn} = \frac{A_{ijNn}}{A_{11Nn}},\\
\bar{B}_{ijNn} = \frac{B_{ijNn}}{A_{11Nn}h_{Nn}}, \bar{D}_{ijNn} = \frac{D_{ijNn}}{A_{11Nn}h_{Nn}^2},\\
\bar{A}_{ijpn} = \frac{A_{ijpn}}{A_{11Nn}}, \bar{A}^*_{ijn} = \frac{A^*_{ijn}}{A_{11Nn}},\\
\bar{B}_{ijpn} = \frac{B_{ijpn}}{A_{11Nn}h_{Nn}}, \bar{B}^*_{ijn} = \frac{B^*_{ijn}}{A_{11Nn}h_{Nn}},\\
\bar{D}_{ijpn} = \frac{D_{ijpn}}{A_{11Nn}h_{Nn}^2}, \bar{D}^*_{ijn} = \frac{D^*_{ijn}}{A_{11Nn}h_{Nn}^2},\\
\bar{F}^*_{11Nn} = \frac{F^*_{11Nn}}{A_{11Nn}h_{Nn}}, \bar{F}^*_{11pn} = \frac{F^*_{11pn}}{A_{11Nn}h_{Nn}},\\
\bar{E}^*_{11Nn} = \frac{E^*_{11Nn}}{A_{11Nn}h_{Nn}^2}, \bar{E}^*_{11pn} = \frac{E^*_{11pn}}{A_{11Nn}h_{Nn}^2},\\
\bar{J}^*_{11Nn} = \frac{J^*_{11Nn}}{\rho_{Nn}h_{Nn}^2}, J^*_{11pn} = \frac{J^*_{11pn}}{\rho_{Nn}h_{Nn}^2},\\
\bar{G}^*_{11Nn} = \frac{G^*_{11Nn}}{\rho_{Nn}h_{Nn}^3}, G^*_{11pn} = \frac{G^*_{11pn}}{\rho_{Nn}h_{Nn}^3},\\
\bar{N}^*_{xpn} = \frac{N^*_{xpn}V_0}{A_{11Nn}}, \bar{N}^*_{\theta pn} = \frac{N^*_{\theta pn}V_0}{A_{11Nn}},\\
\bar{M}^*_{xpn} = \frac{M^*_{xpn}V_0}{A_{11Nn}h_{Nn}}, \bar{M}^*_{\theta pn} = \frac{M^*_{\theta pn}V_0}{A_{11Nn}h_{Nn}},\\
\bar{\tau}^{sn}_0 = \frac{\tau^{sn}_0}{A_{11Nn}}, \bar{R}_n = \frac{R_n}{L}, m_{0n} = \frac{L}{R_n},\\
m_{1n} = \frac{L}{h_{Nn}}, m_{2n} = \frac{h_{Nn}}{R_n} = \bar{h}_{Nn},\\
\bar{h}_{pn} = \frac{h_{pn}}{R_n}, m_{3n} = \frac{I_n}{2\rho_{Nn}h_{Nn}},\\
m_{4n} = \frac{h_{pn}}{h_{Nn}}, \Omega_\mathrm{n} = \sqrt{\frac{A_{11Nn}}{2\rho_{Nn}h_{Nn}L^2}},\\
\tau_n = \Omega_\mathrm{n} t_n, \bar{\omega}_n = \frac{\omega_n}{\Omega_\mathrm{n}}, \bar{K}_w = \frac{K_w L^2}{m_3 A_{11N}},\\
\bar{K}_p = \frac{K_p}{m_3 A_{11N}}, \bar{C}_{w2} = \frac{C_w \Omega L^2}{m_{3n}A_{11Nn}},\\
\bar{C}^L_{vdwn} = \frac{C^L_{vdwn}L^2}{m_{3n}A_{11Nn}},\\
\bar{C}^{NL}_{vdwn} = \frac{C^{NL}_{vdwn}L^2h_{Nn}^2}{m_{3n}A_{11Nn}}, \bar{V}_{DC} = \frac{V_{DC}}{V_0},\\
\bar{V}_{AC} = \frac{V_{AC}}{V_0}, \bar{V}_{p2} = \frac{V_{p2}}{V_0}, \bar{F}_e = \frac{\pi m_1^2 V_0^2 \Upsilon}{m_3 A_{11N}},
\end{gathered} \tag{16}$$

where V_0 is a reference voltage, set to 1 Volt throughout this study [12].

In current study, the electrostatic force Eq. (9) can be expressed as a polynomial form that is solved by nonlinear curve-fitting problem of lsqcurvefit function in Matlab Toolbox using least-squares. Therefore, the dimensionless electrostatic work can be written as follows:

$$W_e = \int_0^L\int_0^{2\pi}\int_0^{\bar{w}_3} \bar{F}_e\left(\begin{array}{c}\bar{V}_{DC}+\\\bar{V}_{AC}\cos(\bar{\omega}\tau)\end{array}\right)^2 \times\left(\begin{array}{c}\bar{C}_1+\bar{C}_2\bar{w}_3\\+\bar{C}_3\bar{w}_3^2+\cdots\\+\bar{C}_n\bar{w}_3^{n-1}\end{array}\right) d\bar{w}_3\,\bar{R}_3 d\theta d\xi \tag{17}$$

which $\bar{C}_1 - \bar{C}_n$ are constant. In according to Figure 2, the nonlinear term of electrostatic force is close to the exact solution for polynomial function with order three and greater. For this figure $R = 1$ nm, $L =$ 10 nm, $h_N = 0.01$ nm and $b = 0.05$ nm are used.

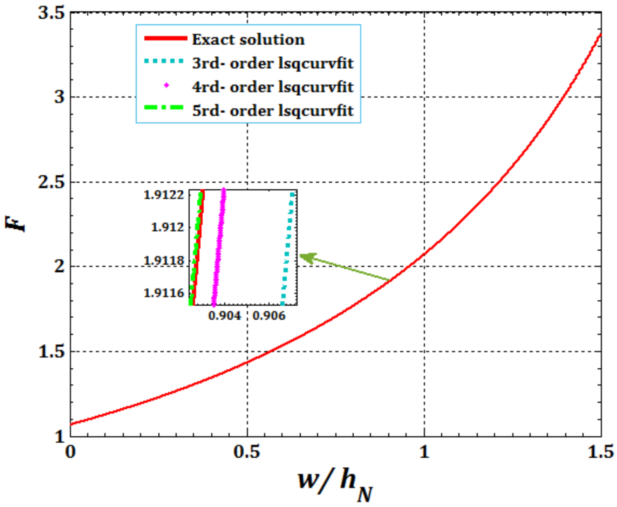

Figure. 2. Comparison between the lsqcurvefit function approximation and the exact value of the nonlinear term of electrostatic force

2.3. Solution procedure

By using the following shear deformation and displacement in the assumed mode method [12, 23]

$$\begin{bmatrix} u_n(x,\theta,t) \\ v_n(x,\theta,t) \\ w_n(x,\theta,t) \end{bmatrix} = \sum_{m=1}^{M_2} \begin{bmatrix} u_{m,0}(\tau)\chi_{m0}(\xi) \\ v_{m,0}(\tau)\phi_{m0}(\xi) \\ w_{m,0}(\tau)\beta_{m0}(\xi) \end{bmatrix} + \sum_{m=1}^{M_1}\sum_{j=1}^{N} \begin{bmatrix} \begin{bmatrix} u_{m,j,c}(\tau)\cos(j\theta) \\ +u_{m,j,s}(\tau)\sin(j\theta) \end{bmatrix}\chi_{mj}(\xi) \\ \begin{bmatrix} v_{m,j,c}(\tau)\sin(j\theta) \\ +v_{m,j,s}(\tau)\cos(j\theta) \end{bmatrix}\phi_{mj}(\xi) \\ \begin{bmatrix} w_{m,j,c}(\tau)\cos(j\theta) \\ +w_{m,j,s}(\tau)\sin(j\theta) \end{bmatrix}\beta_{mj}(\xi) \end{bmatrix} = \sum_{(i,r,s)=1}^{M_2+M_1\times N} \begin{bmatrix} u_{ni}(\tau)\chi_{ni}(\xi)\vartheta_{ni}(\theta) \\ v_{nr}(\tau)\phi_{nr}(\xi)\alpha_{nr}(\theta) \\ w_{ns}(\tau)\beta_{ns}(\xi)\psi_{ns}(\theta) \end{bmatrix}, \quad (18)$$

And using dimensionless strain and kinetic energies Eqs. (5) and (6) and dimensionless applied works Eqs. (7)- (9) and substituting of the Lagrange-Euler equations, the following reduced-order model of the nonlinear equations of motion are obtained:

$$[(M)^u_u]_n\{\ddot{\bar u}_n\} + [(M)^w_u]_n\{\ddot{\bar w}_n\} + [(K)^u_u]_n\{\bar u_n\} + [(K)^v_u]_n\{\bar v_n\} + [(K)^w_u]_n\{\bar w_n\} + [(NL)^w_u]_n\{\bar w_n^2\} = \bar F_{un}, \quad (19)$$

$$[(M)^v_v]_n\{\ddot{\bar v}_n\} + [(M)^w_v]_n\{\ddot{\bar w}_n\} + [(K)^v_v]_n\{\bar v_n\} + [(K)^u_v]_n\{\bar u_n\} + [(K)^w_v]_n\{\bar w_n\}[(NL)^w_v]_n]\{\bar w_n^2\} = \bar F_{vn}, \quad (20)$$

$$\begin{aligned} &\left[[(M)^w_w]_n + \left[(K)^{\ddot w}_{w2}\right]_n\{\bar w_n\}\right]\{\ddot{\bar w}_n\} \\ &+[(c)^w_w]\{\dot{\bar w}_n\} + [(K)^u_w]_n\{\bar u_n\} \\ &+[(K)^v_w]_n\{\bar v_n\} \\ &+[[(K)^w_w]_n - \bar F_{e2}(K_e)^w_w]\{\bar w_n\} \\ &+(-1)^n q_1\left(\frac{\bar R_{n-1}}{\bar R_n}\right)^{m_1} \bar C^{\,L}_{vdw((n-1)n)} \times \\ &\left([(K)^{vdw}_{w1n}]\{\bar w_n\} - [(K)^{vdw}_{w2n}]\{\bar w_{n-1}\}\right) \\ &+(-1)^n q_2\left(\frac{\bar R_n}{\bar R_{n+1}}\right)^{m_2} \bar C^{\,L}_{vdw(n(n+1))} \times \\ &\left([(K)^{vdw}_{w3n}]\{\bar w_{n+1}\} - [(K)^{vdw}_{w4n}]\{\bar w_n\}\right) \\ &+(-1)^n q_1\left(\frac{\bar R_{n-1}}{\bar R_n}\right)^{m_1}\left(\bar C^{\,NL}_{vdw((n-1)n)}\right) \times \\ &\begin{pmatrix} [(NL)^{vdw}_{w1n}]\bar w_n^3 - 3[(NL)^{vdw}_{w2n}]\bar w_n^2\bar w_{n-1} \\ +3[(NL)^{vdw}_{w3n}]\bar w_n\bar w_{n-1}^2 - [(NL)^{vdw}_{w4n}]\bar w_{n-1}^3 \end{pmatrix} \\ &+(-1)^n q_2\left(\frac{\bar R_n}{\bar R_{n+1}}\right)^{m_2}\left(\bar C^{\,NL}_{vdw(n(n+1))}\right) \times \\ &\begin{pmatrix} [(NL)^{vdw}_{w5n}]\bar w_{n+1}^3 - 3[(NL)^{vdw}_{w6n}]\bar w_{n+1}^2\bar w_n \\ +3[(NL)^{vdw}_{w7n}]\bar w_{n+1}\bar w_n^2 - [(NL)^{vdw}_{w8n}]\bar w_n^3 \end{pmatrix} \\ &+[(NL)^u_w]\{\bar w_n\bar u_n\} + [(NL)^v_w]\{\bar w_n\bar v_n\} \\ &+[(NL)^w_{w2} - \bar F_{e3}(NL_{2e})^w_w]\{\bar w_n^2\} \\ &+[(NL)^w_{w3} - \bar F_{e4}(NL_{3e})^w_w]\{\bar w_n^3\} \\ &= \bar F_{we} + \bar F_{wn} \\ &+\bar F_e\left\{\begin{matrix} \begin{pmatrix} (\bar V_{AC}\cos\bar\omega\tau)^2 \\ +2\bar V_{AC}\bar V_{DC}\cos\bar\omega\tau \end{pmatrix} \times \\ \begin{pmatrix} \bar C_4(NL_{3e})^w_w + \bar C_3(NL_{2e})^w_w \\ +\bar C_2(K_e)^w_w + \bar C_1\bar F_1 \end{pmatrix} \end{matrix}\right\} \end{aligned} \quad (21)$$

In Eqs. (19)-(21), for $n=1$: $m_2 = q_1 = 0$; $q_2 = 1$; for $n=2$: $m_2 = 0$; $m_1 = q_1 = 1$; $q_2 = -1$;and for $n=3$: $q_2 = 0; m_1 = 1$; $q_1 = -1$. Also, $[(K)^{vdw}_w]_n$ is stiffness matrix for van der Walls effect. All coefficients of Eqs. (19) - (21) are presented in Appendix 1 and 2.

3. RESULTS AND DISCUSSIONS

In this section, the surface/interface energy effect on the vibration analysis and stability analysis of a MWPENR with arbitrary boundary conditions is investigated. In order to simplify the presentation, C-C, S-S, C-S and C-F represent clamped edge, simply supported edge, clamped-simply supported edge and clamped-free edge, respectively.

The material properties for the different layers of nano-shell (Al) and piezoelectric layer (PZT-4) are shown in Tables 1 and 2 [10].

Table 1. Surface and bulk properties of Al

$E_N(GPa)$	υ_N	$\rho_N(kg/m^3)$	$\lambda^I(N/m)$
70	0.33	2700	3.786
$\mu^I(N/m)$	$\tau_0^I(N/m)$	$\rho^I(kg/m^2)$	
1.95	0.9108	5.46×10^{-7}	

Table 2. Surface and bulk properties of PZT-4

$C_{11p}(GPa)$	$C_{22p}(GPa)$	$C_{12p}(GPa)$
139	139	77.8
$C_{21p}(GPa)$	$C_{66p}(GPa)$	$E_p(GPa)$
77.8	30.5	95
υ_p	$\rho_p(kg\,m^{-3})$	$\eta_{33p}(10^{-8}\,F/m)$
0.3	7500	8.91
$\lambda^S(N/m)$	$\mu^S(N/m)$	$\tau_0^S(N/m)$
4.488	2.774	0.6048
$e_{31p}(C/m^2)$	$e_{32p}(C/m^2)$	$e_{31p}^S(C/m)$
-5.2	-5.2	-3×10^{-8}
$e_{32p}^S(C/m)$	$\rho^S(kg/m^2)$	
-3×10^{-8}	5.61×10^{-6}	

The others geometrical parameters for bulk and surface of MWPENR in all following results are shown in Table 3 [10].

Of course, the geometrical parameters can be varying according to the type of problem. In this work, the results are presented in dimensionless form and thus the results are not limited to a particular type of matter. The data presented in the form of sample data to approximate the values used in the actual range.

Table 3. The material and geometrical parameters.

$R_1(m)$	$R_2(m)$	$R_2(m)$
1×10^{-9}	1.5×10^{-9}	2×10^{-9}
L/R_1	$h_{N_{(1,2,3)}}/R_1$	h_{p_3}/R_1
10	0.01	0.005
b_3/R_3	$K_{w_3}(N/m^3)$	$K_{p_3}(N/m)$
0.1	8.9995035×10^{17}	2.071273
$V_{p_3}(V)$	V_{03}	$V_{AC_3}(V)$
1×10^{-3}	1	10
$V_{DC_3}(V)$	$C_{w_3}(N.S/m)$	$C_{vdw_3}^L(N/m^3)$
15	1×10^{-3}	9.91866693×10^{19}
$C_{vdw_3}^{NL}(N/m^3)$		
2.201667×10^{31}		

3.1. Verification and comparison

In this subsection, the method proposed in this paper is validated by comparing the present results with previously published in the literature of nonclassical theories. In the first case, we compare the results that Ghorbani et al. [30] achieved based on the classic, nonlocal, strain gradient and nonlocal strain gradient theories with and without surface elasticity theory for natural frequencies of SS cylindrical nanoshell with material and geometrical parameters according to Table 4.

Table 4. Material and geometrical parameters for comparison

$E(GPa)$	v	$\rho(kg/m^3)$	$\lambda^s(N/m)$
210	0.24	2331	-4.488
$\mu^s(N/m)$	$\tau_0^s(N/m)$	$\rho_s(kg/m^2)$	$h_N(nm)$
$-2.774\,N$	0.605	3.17×10^{-7}	1
R/h_N	m	n	
2.5	3	3	

In this case, we neglect the nonlinear electrostatic excitation, harmonic force, structural damping and piezoelectric layers. This comparison is presented in Table 5.

Table 5. Comparison of dimensionless natural frequencies calculated based on the present SS nanoshell model and by the model of Ghorbani et al. [30] based on different continuum mechanics theories

Theory	With surface effect		Without surface effect	
	Present study	Ghorbani et al. [30]	Present study	Ghorbani et al. [30]
Classic	0.072453	0.072410	0.017094	0.017016
Nonlocal	0.014042	0.014035	0.003310	0.003298
Strain gradient	0.103102	0.103033	0.024267	0.024213
Nonlocal strain	0.019990	0.019971	0.004734	0.004693

It can be observed from Table 5 that the present results agree very well with the reference solutions, which indicates that the method presented in this paper is suitable and of high accuracy and the insignificant differences in the results may be caused by the different shell theories and solution methodology used in the literature and in this paper.

3.2. Frequency and stability analysis

The main purpose of this section is to obtain dimensionless natural frequency (DNF) and stability analysis considering to the surface/interface effect, piezoelectric voltage, boundary conditions, the length to radius ratio, the nanoresonator gap width and other parameters.

In Figure 3, the effects of all surface and interface parameters is shown on DNF versus different MWPENR length to radius ratio L/R_1 and for two case of surface density corresponding to Table 6 (due to the surface/interface densities play an important role in analysis of natural frequency and nonlinear frequency response).

Table 6. Two case of surface density

Case 1	
$\rho^I(kg/m^2)$	$\rho^S(kg/m^2)$
5.46×10^{-7}	5.61×10^{-6}
Case 2	
$\rho^I(kg/m^2)$	$\rho^S(kg/m^2)$
5.46×10^{-8}	5.61×10^{-7}

It can be seen that with ignoring the surface/interface density $\rho^{(S,I)k}$, the inertia of the system will greatly decrease and due to increasing of MWPENR stiffness, the system will have a maximum DNF compared to other cases.

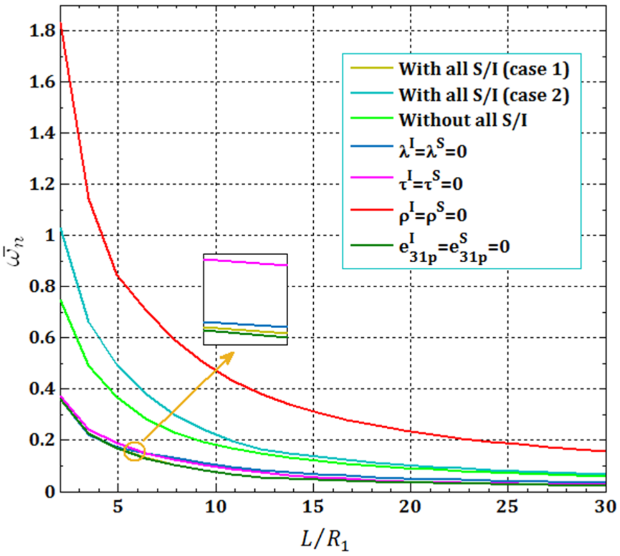

Figure 3. The surface/ interface effects on DNF versus L/R_1 ratio

Also when the surface/interface effects are taken into account corresponding to case 2 of Table 5, due to increasing of nano shell stiffness, it has a higher dimensionless natural frequency than the case of without taking into account all the S/I effects. According to this Figure, regardless the Lamé's constants $\lambda^{(S,I)k}$ and S/I stress ($\tau_0^{(S,I)k}$) slightly lead to increasing of MWPENR stiffness and as a result, the DNF is higher than the case of with all S/I effects (case 1). The surface piezoelectric constants ($e_{31p}^{S_k}$, $e_{32p}^{S_k}$) do not have much effect on the DNF.

The relationship between the DNF and the different MWPENR length to radius ratio L/R_1 is shown in Figure 4 for three vibrational modes. It is observed that for all modes, the DNF decreases when the L/R_1 ratio increases. Also, the DNF for mode 3 is higher than that for modes 1 and 2. It is clear from this Figure that in the case of higher surface/interface densities (case 1), the inertia of the shell is increased and its stiffness is reduced that leads to decreasing of the DNF compared to case of without S/I effects. Also, with decreasing of surface/interface densities (case 2), the inertia of the system is increased and with increase of stiffness, DNF increases compared to case of without S/I effects.

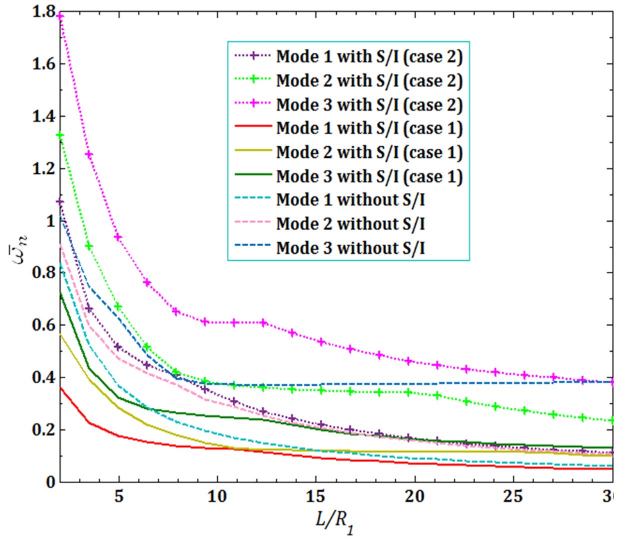

Figure 4. The surface/ interface effects on DNF versus L/R_1 ratio for three vibrational modes

Dimensionless natural frequencies of MWPENR versus L/R_1 ratio with and without surface/interface (S/I densities case 2) is presented in Figures 5. It is clear from the Figure 5 that in all boundary conditions, higher surface/interface densities (case 1) leads to reduction of MWPENR stiffness, as a result cause to decreasing of the dimensionless natural frequency compared to case of without S/I effects. Also, with decreasing of surface/interface densities (case 2) and as a result increasing of the MWPENR stiffness, the dimensionless natural frequency is increased compared to case of without S/I effects.

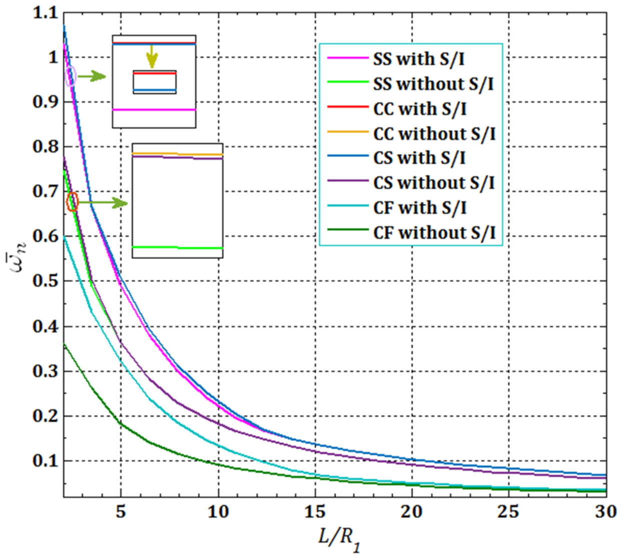

Figure 5. The surface/ interface effects on natural frequency versus L/R_1 ratio for different boundary conditions

Figure 6 show the influence of the SS MWPENR piezoelectric actuation voltages $\bar{V}_p$ on DNF versus different MWPENR length to radius ratio L/R_1 with all surface/ interface effects. As can be seen from Figure, voltage $\bar{V}_p$ can remarkably influence on DNF and with increasing of this voltage, due to increasing of MWPENR stiffness, DNF will increase.

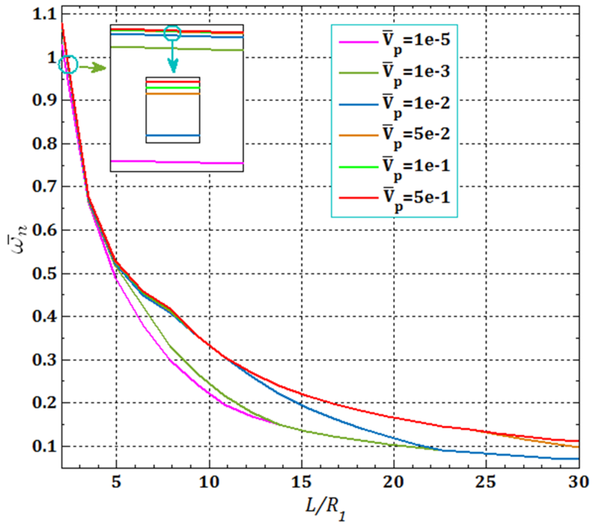

Figure 6. The effects of the piezoelectric voltage $\bar{V}_p$ on DNF versus L/R_1 with all S/I effects

The effect of direct pull in voltage DC on the natural frequency of MWPENR for different boundary conditions is presented in Figure 7. It can be seen that the CC boundary condition with S/I (case2) has the highest natural frequency and the CF boundary condition without S/I has the lowest natural frequency. In all boundary conditions, with S/I (case 2) have maximum natural frequency and pull in voltage. In this case, with decreasing of surface/interface densities, the inertia of the system is increased and with increase of stiffness, natural frequency is increased, accordingly the natural frequency is increased compared to case of without S/I effects.

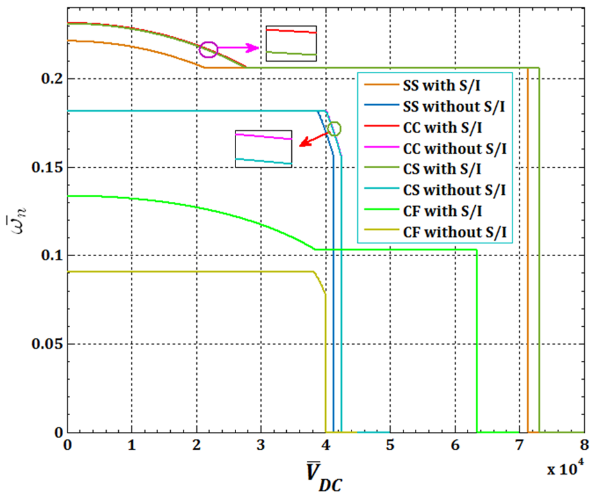

Figure 7. The effect of direct pull in voltage DC on the natural frequency of MWPENR for different boundary conditions

The influence of different the nanoresonator gap distance ratio b/R_3 and the length to radius ratio L/R_3 on the natural frequency and pull-in instability of SS MWPENR is presented respectively in Figure 8 and 9. It is clear from this Figure that with increasing of b/R_3 ratio and decreasing of L/R_3 ratio, due to increasing of MWPENR stiffness, the pull-in voltages of the piezoelectric nanoresonator is increased. In addition, it is found that, the natural frequency of actuated SS MWPENR decreases by increasing the applied voltage until the natural frequency vanishes and the nanoresonator drops to the rigid gate.

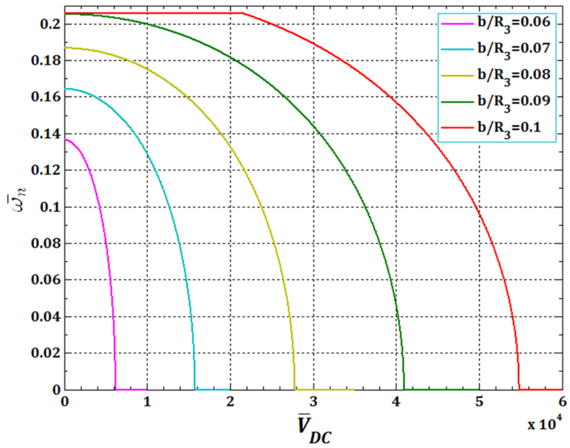

Figure 8. The effect of direct pull in voltage DC on the fundamental frequency of SS MWPENR for different b/R ratio

Also, for zero natural frequency, SS MWPENR becomes unstable and the corresponding voltage is called the critical voltage named pull in voltage. For example, in Figure 8, natural frequency to the lower value of $b/R_3 = 0.06$ sooner than the rest values of this ratio is reached to be zero. This physically implies that first the PENR in $b/R_2 = 0.06$ losses its stability due to the divergence via a pitchfork bifurcation.

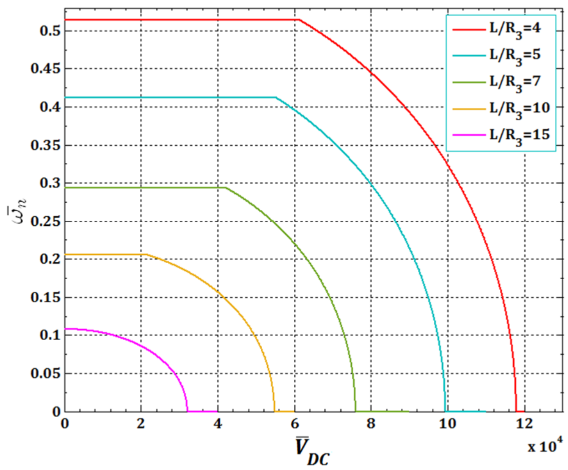

Figure 9. The effect of direct pull in voltage DC on the fundamental frequency of SS MWPENR for different values of L/R_1 ratio

Figure 10 show the influence of the piezoelectric actuation voltages $\bar{V}_p$ on the pull in voltage of SS MWPENR, while varying the DC voltage. As can be seen from Figure, voltage $\bar{V}_p$ can remarkably influence the pull-in voltages. As it is shown in Figure 10, by increasing the applied voltage to the piezoelectric layers, the piezoelectric nanoresonator stiffens and technically the pull-in voltage increases by softening the SS MWPENR.

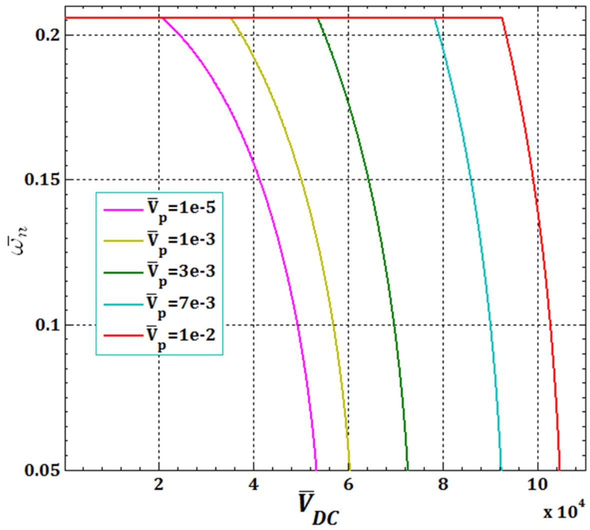

Figure 10. Influence of the piezoelectric voltage $\bar{V}_p$ on the fundamental frequency of SS PENR versus the direct pull in voltage DC

It is noted that piezoelectric actuation can be considered as a design parameter to control the system pull-in instability.

Figure 11 show the comparison of three nonclassical theories of NLT, NSGT (For more information on these methods, refer to reference [9]) and GMSIT with classical theory CT on dimensionless natural frequency versus ratio L/R_1 for SS MWPENS. It can be seen from this Figure that the highest frequency is related to the GMSIT and shows that in this case, the system's rigidity is higher than other cases. The lowest frequency is also related to nonlocal theory NL and shows that in this case, the system hardness is less than other cases. Also, the natural frequency of the classical theory is greater than the NLT, NSGT and combination of GMSIT+NLT and GMSIT+NSGT theories, indicating a reduction in the rigidity of the system due to the consideration of these theories. This results shown that S/I effects lead to increasing of MWPENS stiffness and other nonclassical effects lead to decreasing of MWPENS stiffness and as a result decreasing of DNF.

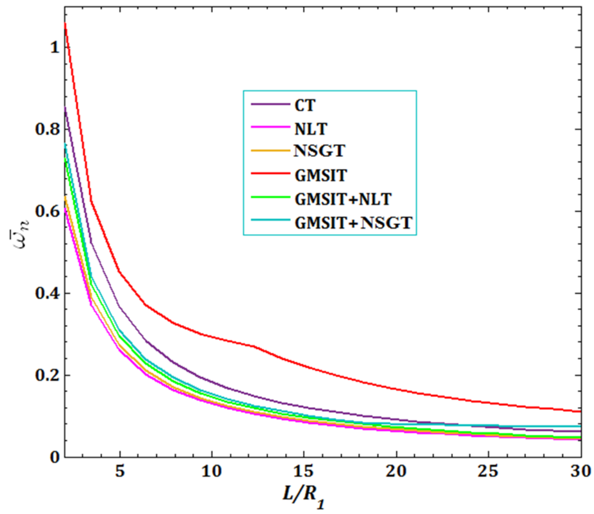

Figure 11. Comparison of nonclassical theories with classical theory on dimensionless natural frequency versus SS MWPENS L/R_1 ratio

Figure 12 shows the comparison of three nonclassical theories of NLT, NSGT and GMSIT with classical theory CT on dimensionless natural frequency versus different piezoelectric actuation voltage $\bar{V}_p$ for SS MWPENS.

All of the results presented in the previous Figure on the effects of various theories on natural frequencies are clearly seen in this Figure and confirm the previous results. In all case, with increasing of piezoelectric voltage and as a result increasing the rigidity of the system, the frequency increases. In theories of CT, GMSIT, GMSIT+NLT GMSIT+NSGT, the frequency increases and by most increasing of $\bar{V}_p$, piezoelectric voltage variations do not have a significant effect on the natural frequency of the MWPENS. But in NLT and NSGT, with increasing of $\bar{V}_p$, DNF increases with slightly slop and by most increasing of $\bar{V}_p$, this increasing of DNF considerable.

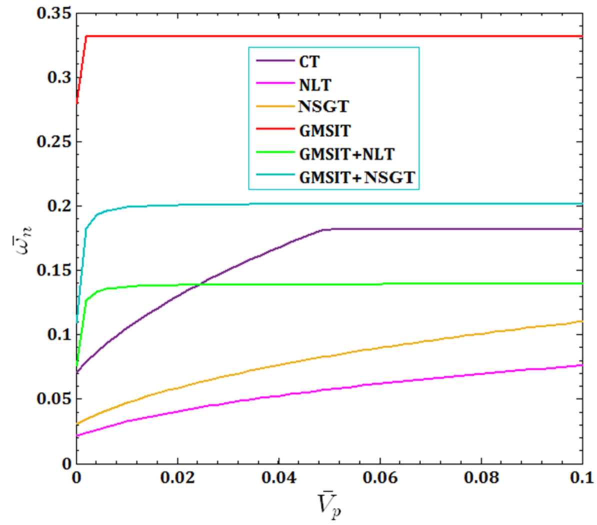

Figure 12. Comparison of nonclassical theories with classical theory on dimensionless natural frequency versus different piezoelectric voltage $\bar{V}_p$

4. CONCLUSION

In current study, vibration and stability analysis of multi walled piezoelectric nanoresonator based on cylindrical nano-shell is investigated using using three nonclassical theories of nonlocal, nonlocal strain gradient and Gurtin–Murdoch surface/interface. The nanoresonator is embedded in visco-Pasternak medium, the nonlinear van der Waals (vdW) and electrostatic forces. Hamilton's principle is used for deriving of the governing equations and boundary conditions and also the assumed mode method is used for changing the partial differential equations into ordinary differential equation. The influences of the surface/interface effect, piezoelectric voltage, boundary conditions, the length to radius ratio, the nanoresonator gap width and other parameters are studied on the frequency and stability analysis of MWPENR.

Some conclusions obtained from this study are:

- with ignoring the surface/interface density $\rho^{(S,I)k}$, the inertia of the system will greatly decrease and due to increasing of MWPENR stiffness, the system will have a maximum DNF compared to other cases.
- when the surface/interface effects are taken into account corresponding to case 2, due to increasing of nano shell stiffness, it has a higher dimensionless natural frequency than the case of without all S/I effects.
- Regardless the Lamé's constants $\lambda^{(S,I)k}$ and S/I stress ($\tau_0^{(S,I)k}$) slightly lead to increasing of MWPENR stiffness and as a result, the DNF is higher than the case of with all S/I effects (case 1).
- The surface piezoelectric constants ($e_{31p}^{s_k}, e_{32p}^{s_k}$) do not have much effect on the DNF.
- for all modes, the DNF decreases when the L/R_1 ratio increases. Also, the DNF for mode 3 is higher than that for modes 1 and 2.
- in all boundary conditions, higher surface/interface densities lead to reduction of MWPENR stiffness, as a result cause to decreasing of the dimensionless natural frequency compared to case of without S/I effects.
- with decreasing of surface/interface densities and as a result increasing of the MWPENR stiffness, the dimensionless natural frequency is increased compared to case of without S/I effects.
- voltage $\bar{V}_p$ can remarkably influence on DNF and with increasing of this voltage, due to increasing of MWPENR stiffness, DNF will increase.
- the CC boundary condition with S/I has the highest natural frequency and the CF boundary condition without S/I has the lowest natural frequency.
- In all boundary conditions, with S/I have maximum natural frequency and pull in voltage. In this case, with decreasing of surface/interface densities, the inertia of the system is increased and with increase of stiffness, natural frequency is increased, accordingly the natural frequency is increased compared to case of without S/I effects.
- with increasing of b/R_3 ratio and decreasing of L/R_3 ratio, due to increasing of MWPENR stiffness, the pull-in voltages of the piezoelectric nanoresonator is increased.
- the natural frequency of actuated SS MWPENR decreases by increasing the applied voltage until the natural frequency vanishes and the nanoresonator drops to the rigid gate.
- by increasing the applied voltage to the piezoelectric layers $\bar{V}_p$, the piezoelectric nanoresonator stiffens and technically the pull-in voltage increases by softening the SS MWPENR.
- Nonlocal scale parameter $\bar{\mu}$, material length scale parameter $\bar{\eta}$ and pull-in voltage DC respectively lead to increasing and decreasing of MWPENS stiffness and results of lead to increasing and decreasing the DNF of MWPENS.
- the highest frequency is related to the GMSIT and shows that in this case, the system's rigidity is higher than other cases.
- the lowest frequency is also related to nonlocal theory NL and shows that in this case, the system hardness is less than other cases.
- the natural frequency of the classical theory is greater than the NLT, NSGT and combination of GMSIT+NLT and GMSIT+NSGT theories.
- with increasing of piezoelectric voltage in all theories, due to increasing the rigidity of the system, the frequency increases.

CONFLICT OF INTEREST

The authors report no conflict of interest.

FUNDING ACKNOWLEDGEMENT

'This research received no specific grant from any funding agency in the public, commercial, or not-for-profit sectors'.

REFERENCES

[1] Tichý J., Erhart J., Kittinger E., Prívratská J., *Fundamentals of Piezoelectric Sensorics; Mechanical, Dielectric, and Thermodynamical Properties of Piezoelectric Materials*, Springer, 2010.

[2] Fang X.Q., Liu J.X., Gupta V., Fundamental formulations and recent achievements in piezoelectric nano-structures: a review, *Nanoscale*, Vol. 5, 2013, 1716.

[3] Tzou H., *Piezoelectric Shells: Sensing, Energy Harvesting, and Distributed Control*, Springer, 2019.
[4] Gurtin M.E., Murdoch A.I., Surface stress in solids, *International Journal of Solids and Structures*, Vol. 14, 1978, pp. 431–40.
[5] Hajnayeb A., Khadem S.E., Nonlinear vibration and stability analysis of a double-walled carbon nanotube under electrostatic actuation, *Journal of Sound and Vibration*, Vol.331, 2012, pp. 2443–2456.
[6] Ghorbanpour Arani A., Kolahchi R., Khoddami Maraghi Z., Nonlinear vibration and instability of embedded double-walled boron nitride nanotubes based on nonlocal cylindrical shell theory, *Applied Mathematical Modelling*, Vol. 37, 2013), pp. 7685–7707.
[7] Ghorbanpour Arani A., Amir S., A Shajari.R., Mozdianfard M.R., Electro-thermo-mechanical buckling of DWBNNTs embedded in bundle of CNTs using nonlocal piezoelasticity cylindrical shell theory, *Composites: Part B*, Vol. 43, 2012, pp. 195–203.
[8] Tadi Beni Y., Koochi A., Abadyan M., Using modified couple stress theory for modeling the size-dependent pull-in instability of torsional nano-mirror under Casimir force. *International Journal of Optomechatronics*, Vol. 8, 2014, pp. 47-71.
[9] Hashemi Kachapi S.H., Nonlinear vibration and stability analysis of piezo-harmo-electrostatic nanoresonator based on surface/interface and nonlocal strain gradient effects, *Journal of the Brazilian Society of Mechanical Sciences and Engineering*, Vol. 42, 2020, DOI:10.1007/s40430-020-2173-1.
[10] Hashemi Kachapi S.H., Nonlinear vibration and stability analysis of double-walled piezoelectric nanoresonator with nonlinear van der Waals and electrostatic excitation, *Journal of Vibration and Control*, Vol. 26, 2020, pp. 680–700.
[11] Hashemi Kachapi S.H., Dardel M., Mohamadi daniali H., Fathi A., Effects of surface energy on vibration characteristics of double-walled piezo-viscoelastic cylindrical nanoshel, *Proceedings of the Institution of Mechanical Engineers, Part C: Journal of Mechanical Engineering Science*, 2019, DOI: 10.1177/0954406219845019.
[12] Hashemi Kachapi S.H., Dardel M., Mohamadi daniali H., Fathi A., Pull-in instability and nonlinear vibration analysis of electrostatically piezoelectric nanoresonator with surface/interface effects, *Thin-Walled Structures*, Vol. 143, 2019, pp. 106210.
[13] Hashemi Kachapi S.H., Dardel M., Mohamadi daniali H., Fathi A., Nonlinear dynamics and stability analysis of piezo-visco medium nanoshell resonator with electrostatic and harmonic actuation, *Applied Mathematical Modelling*, 2019, DOI:10.1016/j.apm.2019.05.035.
[14] Hashemi Kachapi S.H., Dardel M., Mohamadi daniali H., Fathi A., Nonlinear dynamic response and frequency analysis of the FG-PCNS with surface energy effects, *Romanian Journal of Acoustics and Vibration*, Vol. 16, No. 1, 2019, pp. 15-31.
[15] Phung-Van, P., Thai, Chien. H., Nguyen-Xuan, H., Abdel Wahab, M., Porosity-dependent nonlinear transient responses of functionally graded nanoplates using isogeometric analysis, *Composites Part B: Engineering*, Vol. 164, 2019, pp. 215-225.
[16] Thanh, Cuong-Le, Phung-Van, P., Thai, Chien H., Nguyen-Xuan, H., Abdel Wahab, M., Isogeometric analysis of functionally graded carbon nanotube reinforced composite nanoplates using modified couple stress theory, *Composite Structures*, Vol. 184, 2018, 633-649.
[17] Thanh, Cuong-Le, Ferreira, A.J.M., Abdel Wahab, M., A refined size-dependent couple stress theory for laminated composite micro-plates using isogeometric analysis, *Thin-Walled Structures*, Vol. 145, 2019, 106427.
[18] Thanh, Cuong-Le, Tran, Loc V., Vu-Huu, T., Abdel-Wahab, M., The size-dependent thermal bending and buckling analyses of composite laminate microplate based on new modified couple stress theory and isogeometric analysis, *Computer Methods in Applied Mechanics and Engineering*, Vol. 350, 2019, pp. 337-361.
[19] Thanh, Cuong-Le, Tran, Loc V., Vu-Huu, T., Nguyen-Xuan, H., Abdel-Wahab, M., Size-dependent nonlinear analysis and damping responses of FG-CNTRC micro-plates, *Methods in Applied Mechanics and Engineering*, Vol. 353, 2019, pp. 253-276.
[20] Phung-Van, P., Thanh, Cuong-Le, Nguyen-Xuan, H., Abdel-Wahab, M., Nonlinear transient isogeometric analysis of FG-CNTRC nanoplates in thermal environments, *Composite Structures*, vol. 201, 2018, pp. 882-892.
[21] Phung-Van, P., Tran, Loc V., Ferreira, AJM., Nguyen-Xuan, H., Abdel Wahab, M., Nonlinear transient isogeometric analysis of smart piezoelectric functionally graded material plates based on generalized shear deformation theory under thermo-electro-mechanical loads, *Nonlinear dynamics*, Vol. 87, 2017, pp.879-894.
[22] Donnell L. H., *Beam, Plates and Shells*, McGraw-Hill, 1976.
[23] Amabili M., *Nonlinear Vibrations and Stability of Shells and Plates*, Cambridge University Press, 2008.
[24] Sabzikar Boroujerdy M., Eslami M.R., Axisymmetric snap-through behavior of Piezo-FGM shallow clamped spherical shells under thermo-electro-mechanical loading, *International Journal of Pressure Vessels and Piping*, Vol. 120-121, 2014, pp. 19-26.
[25] Kirchhoff G., Über das Gleichgewicht und die Bewegung einer elastischen Scheibe, *Journal fur reine und angewandte Mathematik*, Vol. 40, 1850, pp. 51-88.
[26] Lu P., He L.H., Lee H.P., Lu C., Thin plate theory including surface effects, *International Journal of Solids and Structures*, Vol. 43, 2006, pp. 4631–47.
[27] Ke L.L., Wang Y.S., Reddy J.N., Thermo-electro-mechanical vibration of size-dependent piezoelectric cylindrical nanoshells under various boundary conditions, *Composite Structures*, Vol. 116, 2014, pp. 626-636.
[28] Jafari S. B., Malekfar R., Khadem S. E., Radial Breathing Mode Frequency of Multi-Walled Carbon Nanotube Via Multiple-Elastic Thin Shell Theory, *International Journal of Nanoscience and Nanotechnology*, Vol. 7, 2011, pp. 137-142.
[29] He X. Q., Kitipornchai S., Liew K. M., Buckling Analysis of Multi-Walled Carbon Nanotubes: A Continuum Model Accounting for Van Der Waals Interaction, *Journal of the Mechanics and Physics of Solids*, Vol. 53, 2005, pp. 303–326.
[30] Ghorbani K., Mohammadi K., Rajabpour A., Ghadiri M., Surface and size-dependent effects on the free vibration analysis of cylindrical shell based on Gurtin-Murdoch and nonlocal strain gradient theories, *Journal of Physics and Chemistry of Solids*. Vol. 129, 2019, pp. 140-150.

APPENDIX 1

$\alpha_{1n} = \frac{1}{m_{3n}} \bar{A}_{11n}$, $\alpha_{2n} = \frac{m_{0n}^2}{m_{3n}} \bar{A}_{66n}$,

$\alpha_{3n} = \frac{m_{0n}}{m_{3n}} (\bar{A}_{12n} + \bar{A}_{21n})$, $\alpha_{4n} = \frac{2m_{0n}}{m_{3n}} \bar{A}_{66n}$,

$\alpha_{5n} = \frac{m_{0n}}{m_{3n}} (\bar{A}_{12n} + \bar{A}_{21n})$,

$\alpha_{6n} = \frac{1}{m_{1n} m_{3n}} \left(\bar{A}_{11n} - \bar{\tau}_{0n}^{ps} - \bar{\tau}_{0n}^{NI}\right)$,

$\alpha_{7n} = \frac{m_{0n} m_{2n}}{2m_{3n}} (\bar{A}_{12n} + \bar{A}_{21n})$,

$\alpha_{8n} = \frac{2m_{0n} m_{2n}}{m_{3n}} \bar{A}_{66n}$, $\alpha_{9n} = \frac{m_{0n}^2}{m_{3n}} \bar{A}_{22n}$,

$\alpha_{10n} = \frac{m_{0n}^2 m_{2n}}{m_{3n}} \left(\bar{A}_{22n} - \bar{\tau}_{0n}^{ps} - \bar{\tau}_{0n}^{NI}\right)$,

$\alpha_{11n} = \frac{m_{2n}}{2m_{3n}} (\bar{A}_{12n} + \bar{A}_{21n})$,

$\alpha_{12n} = \frac{2m_{0n}^2}{m_{3n}} \left(\bar{A}_{22n} - \bar{\tau}_{0n}^{ps} - \bar{\tau}_{0n}^{NI}\right)$,

$\alpha_{13n} = \frac{1}{m_{3n}} \bar{A}_{66n}$, $\alpha_{14n} = \frac{2m_{2n}}{m_{3n}} \bar{A}_{66n}$,

$\alpha_{15n} = \frac{m_{0n}^2}{m_{3n}} \left(\bar{A}_{22n} - 2\left(\bar{\tau}_{0n}^{ps} + \bar{\tau}_{0n}^{NI}\right)\right)$,

$\alpha_{16n} = \frac{1}{4m_{1n}^2 m_{3n}} \left(\bar{A}_{11n} - 2\left(\bar{\tau}_{0n}^{ps} + \bar{\tau}_{0n}^{NI}\right)\right)$,

$\alpha_{17n} = \frac{m_{0n}^2 m_{2n}^2}{4m_{3n}} \left(\bar{A}_{22n} - 2\left(\bar{\tau}_{0n}^{ps} + \bar{\tau}_{0n}^{NI}\right)\right)$,

$\alpha_{18n} = \frac{m_{2n}^2}{4m_{3n}} (4\bar{A}_{66n} + \bar{A}_{12n} + \bar{A}_{21n})$,

$\alpha_{19n} = \frac{m_{2n}}{2m_{3n}} (\bar{A}_{12n} + \bar{A}_{21n})$,

$\alpha_{20n} = \frac{m_{0n}^2 m_{2n}}{m_{3n}} \left(\bar{A}_{22n} - 2\left(\bar{\tau}_{0n}^{ps} + \bar{\tau}_{0n}^{NI}\right)\right)$,

$\alpha_{21n} = \frac{1}{m_{1n}^2 m_{3n}} (\bar{D}_{11n} - \bar{E}_{11n})$,

$\alpha_{22n} = \frac{m_{0n}^2 m_{2n}^2}{m_{3n}} (\bar{D}_{22n} - \bar{E}_{11n})$,

$\alpha_{23n} = \frac{4m_{2n}^2}{m_{3n}} \bar{D}_{66n}$,

$\alpha_{24n} = \frac{m_{2n}^2}{m_{3n}} (\bar{D}_{12n} + \bar{D}_{21n} - 2\bar{E}_{11n})$,

$\alpha_{25n} = \frac{m_{0n} m_{1n}}{m_{3n}} \left(2\left(\bar{\tau}_{0n}^{ps} + \bar{\tau}_{0n}^{NI}\right) - \bar{N}_{\theta pn}\right)$,

$\alpha_{26n} = \frac{m_{1n}}{m_{3n}} \left(2\left(\bar{\tau}_{0n}^{ps} + \bar{\tau}_{0n}^{NI}\right) - \bar{N}_{xpn}\right)$,

$\alpha_{27n} = \frac{m_{0n} m_{1n}}{m_{3n}} \left(2\left(\bar{\tau}_{0n}^{ps} + \bar{\tau}_{0n}^{NI}\right) - \bar{N}_{\theta pn}\right)$,

$\alpha_{28n} = \frac{1}{2m_{3n}} \left(2\left(\bar{\tau}_{0n}^{ps} + \bar{\tau}_{0n}^{NI}\right) - \bar{N}_{xpn}\right)$,

$\alpha_{29n} = \frac{m_{0n}^2}{2m_{3n}} \left(2\left(\bar{\tau}_{0n}^{ps} + \bar{\tau}_{0n}^{NI}\right) - \bar{N}_{\theta pn}\right)$,

$\alpha_{30n} = \frac{1}{m_{3n}} \bar{M}_{xpn}$, $\alpha_{31n} = \frac{m_{0n}^2}{m_{3n}} \bar{M}_{\theta pn}$,

$\alpha_{32n} = \frac{1}{2m_{1n}^2 m_{3n}} \bar{G}_{11n}^*$, $\alpha_{33n} = \frac{m_{2n}^2}{2m_{3n}} \bar{G}_{11n}^*$,

APPENDIX 2

$(M)_{un}^u = \iint \left(\chi_e \chi_i \vartheta_f \vartheta_j\right) d\xi\, d\theta$,

$(K)_{un}^u = \iint \begin{pmatrix} \alpha_{1n} \chi_e' \chi_i' \vartheta_f \vartheta_j \\ +\alpha_{2n} \chi_e \chi_i \vartheta_f' \vartheta_j' \end{pmatrix} d\xi\, d\theta$,

$(K)_{un}^v = \frac{1}{2} \iint \begin{pmatrix} \alpha_{3n} \chi_e' \phi_k \vartheta_f \alpha_l' \\ +\alpha_{4n} \chi_e \phi_k' \vartheta_f' \alpha_l \end{pmatrix} d\xi\, d\theta$,

$(K)_{un}^w = \frac{1}{2} \iint \left(\alpha_{5n} \chi_e' \beta_o \vartheta_f \psi_l\right) d\xi\, d\theta$,

$(NL)_{un}^w = \frac{1}{2} \iint \begin{pmatrix} \alpha_{6n} \chi_e' \beta_0' \beta_t' \vartheta_f \psi_p \psi_v \\ +\alpha_{7n} \chi_e' \beta_o \beta_t \vartheta_f \psi_p' \psi_v' \\ +\alpha_{8n} \chi_e \beta_0' \beta_t \vartheta_f' \psi_p \psi_v' \end{pmatrix} d\xi\, d\theta$,

$\bar{F}_{upn} = \frac{1}{2} \iint \left(\alpha_{26n} \chi_e' \vartheta_i\right) d\xi\, d\theta$,

$(M)_{vn}^v = \iint \left(\phi_q \phi_k \alpha_f \alpha_l\right) d\xi\, d\theta$

$(K)_{vn}^u = \frac{1}{2} \iint \begin{pmatrix} \alpha_{3n} \phi_q \chi_i' \alpha_f' \vartheta_l \\ +\alpha_{4n} \phi_q' \chi_i \alpha_f \vartheta_l' \end{pmatrix} d\xi\, d\theta$,

$(K)_{vn}^v = \iint \begin{pmatrix} \alpha_{9n} \phi_q \phi_k \alpha_f' \alpha_l' \\ +\alpha_{13n} \phi_q' \phi_k' \alpha_f \alpha_l \end{pmatrix} d\xi\, d\theta$,

$(K)_{vn}^w = \frac{1}{2} \iint \left(\alpha_{12n} \phi_q \beta_o \alpha_f' \psi_l\right) d\xi\, d\theta$,

$(NL)_{vn}^w = \frac{1}{2} \iint \begin{pmatrix} \alpha_{10n} \phi_q \beta_o \beta_t \alpha_g' \psi_p' \psi_v' \\ +\alpha_{11n} \phi_q \beta_0' \beta_t' \alpha_g' \psi_p \psi_v \\ +\alpha_{14n} \phi_q' \beta_0' \beta_t \alpha_g \psi_p \psi_v' \end{pmatrix} d\xi\, d\theta$,

$\bar{F}_{vpn} = \frac{1}{2} \iint \left(\alpha_{27n} \phi_q \alpha_f'\right) d\xi\, d\theta$,

$(M)_{wn}^w = \frac{1}{2} \iint \begin{pmatrix} 2\beta_r \beta_o \psi_s \psi_p \\ +\alpha_{32n} \beta_r'' \beta_o \psi_s \psi_p \\ +\alpha_{33n} \beta_r \beta_o \psi_s'' \psi_p \end{pmatrix} d\xi\, d\theta$,

$(C)_{wn}^w = \frac{1}{2} \iint \left(\bar{C}_{wn} \beta_r \beta_o \psi_s \psi_p\right) d\xi\, d\theta$,

$(K)_{wn}^u = \frac{1}{2} \iint \left(\alpha_{5n} \beta_r \chi_i' \psi_s \vartheta_j\right) d\xi\, d\theta$,

$(K)_{wn}^v = \frac{1}{2} \iint \left(\alpha_{12n} \beta_r \phi_k \psi_s \alpha_l'\right) d\xi\, d\theta$,

$$(K)_{wn}^w = \frac{1}{2} \times \iint \begin{pmatrix} 2\alpha_{15n} \beta_r \beta_o \psi_s \psi_p + 2\alpha_{21n} \beta_r'' \beta_0'' \psi_s \psi_p \\ +2\alpha_{22n} \beta_o \beta_r \psi_s'' \psi_p'' + 2\alpha_{23n} \beta_r' \beta_o' \psi_s' \psi_p' \\ +\alpha_{24n} \beta_r \beta_o'' \psi_s'' \psi_p + \alpha_{24n} \beta_r'' \beta_o \psi_s \psi_p'' \\ +2\alpha_{28n} \beta_r' \beta_o' \psi_s \psi_p + \bar{k}_w \beta_r \beta_o \psi_s \psi_p \\ -\bar{k}_p \beta_r \beta_0'' \psi_s \psi_p - \bar{k}_p m_0^2 \beta_r \beta_o \psi_s \psi_p'' \\ -\bar{F}_{e2} (K_e)_w^w \end{pmatrix} d\xi\, d\theta,$$

$(K_e)_{wn}^w = \beta_r \beta_o \psi_s \psi_p$,

$(K)_{win}^{vdw} = \frac{1}{2} \iint \left(\beta_r \beta_o \psi_s \psi_p\right) d\xi\, d\theta$,

$i = 1 \ldots 4$,

$$(NL)_{wn}^{u}=\frac{1}{2}\times$$
$$\iint \begin{pmatrix} 2\alpha_{6n}\beta_r'\beta_o'\chi_i'\psi_s\psi_p\vartheta_j+2\alpha_{7n}\beta_r\beta_o\chi_i'\psi_s'\psi_p'\vartheta_j \\ +\alpha_{8n}\beta_r'\beta_o\chi_i\psi_s\psi_p'\vartheta_j'+\alpha_{8n}\beta_r\beta_o'\chi_i\psi_s'\psi_p\vartheta_j' \end{pmatrix} d\xi\, d\theta,$$
$$(NL)_{wn}^{v}=\frac{1}{2}\times$$
$$\iint \begin{pmatrix} 2\alpha_{10n}\beta_r\beta_o\phi_k\psi_s'\psi_p'\alpha_l'+2\alpha_{11n}\beta_r'\beta_o'\phi_k\psi_s\psi_p\alpha_l' \\ +\alpha_{14n}\beta_r'\beta_o\phi_k'\psi_s\psi_p'\alpha_l+\alpha_{14n}\beta_r\beta_o'\phi_k'\psi_s'\psi_p\alpha_l \end{pmatrix} d\xi\, d\theta,$$
$$(NL)_{w2n}^{w}=\frac{1}{2}\times$$
$$\iint \begin{pmatrix} \alpha_{19n}\beta_r\beta_o'\beta_t'\psi_s\psi_p\psi_v+2\alpha_{19n}\beta_r'\beta_o'\beta_t\psi_s\psi_p\psi_v \\ +\alpha_{20n}\beta_r\beta_o\beta_t\psi_s\psi_p'\psi_v' \\ +2\alpha_{20n}\beta_r\beta_o\beta_t\psi_s'\psi_p'\psi_v-\bar{F}_{e3}(NL_{2e})_w^w \end{pmatrix} d\xi\, d\theta\ ,$$
$$(NL_{2e})_{wn}^{w}=\beta_r\beta_o\beta_t\psi_s\psi_p\psi_v,$$
$$(NL)_{w3n}^{w}=\frac{1}{2}\times$$
$$\iint \begin{pmatrix} 4\alpha_{16n}\beta_r'\beta_o'\beta_t'\beta_a'\psi_s\psi_p\psi_v\psi_b \\ +4\alpha_{17n}\beta_r\beta_o\beta_t\beta_a\psi_s'\psi_p'\psi_v'\psi_b' \\ +2\alpha_{18n}\beta_r'\beta_o'\beta_t\beta_a\psi_s\psi_p\psi_v'\psi_b' \\ +2\alpha_{18n}\beta_r\beta_o\beta_t'\beta_a'\psi_s'\psi_p'\psi_v\psi_b \\ -\bar{F}_{e4}(NL_{3e})_w^w \end{pmatrix} d\xi\, d\theta$$
$$(NL_{3e})_{wn}^{w}=\beta_r\beta_o\beta_t\beta_a\psi_s\psi_p\psi_v\psi_b$$
$$(NL)_{win}^{vdw}=\frac{1}{2}\iint \left(\beta_r\beta_o\beta_t\beta_a\psi_s\psi_p\psi_v\psi_b\right)d\xi d\theta,$$
$$i=1\dots 4,$$
$$\bar{F}_{wp}=\frac{1}{2}\iint \begin{pmatrix} \alpha_{25}\beta_r\psi_s+\alpha_{30}\beta_r''\psi_s \\ +\alpha_{31}\beta_r\psi_s'' \end{pmatrix} d\xi\, d\theta,$$
$$\bar{F}_1=\iint (\beta_r\psi_s)d\xi\, d\theta\ ,$$
$$\bar{F}_{e1}=\frac{1}{2}\bar{F}_e\bar{F}_1,\ \ \bar{F}_{eDC}=\frac{1}{2}\bar{F}_e\bar{V}_{DC}^2,$$
$$\bar{F}_{we}=\bar{C}_1\bar{F}_{eDC}\bar{F}_1,\ \ \bar{F}_{e2}=\bar{C}_2\bar{F}_{eDC},$$
$$\bar{F}_{e3}=\bar{C}_3\bar{F}_{eDC},\bar{F}_{e4}=\bar{C}_4\bar{F}_{eDC},$$